Supporting Information: A structural perspective on the dynamics of kinesin motors

Changbong Hyeon[1]
School of Computational Sciences,
Korea Institute for Advanced Study, Seoul 130-722, Republic of Korea

José N. Onuchic[2]
Center for Theoretical Biological Physics and Department of Physics,
University of California at San Diego, La Jolla, California 92093-0374, USA

[1]Email: hyeoncb@kias.re.kr
[2]Email: jonuchic@rice.edu

Operational conditions for biological machines

In the macroworld, the length, time, and energy scales of an object are well-separated from its surrounding, thus conventional Newtonian mechanics can determine the trajectory of the object deterministically. Such separation of scales, however, does not hold as the object size is reduced to nanoscales where the effect of thermal noise from the surrounding is substantial. While the thermal noise imparts incessant fluctuation to the molecule and hinders precise measurement, the thermal noise is an essential component to trigger the conformational changes of biological motors. Below we illuminate the general design principles of molecular machines by contrasting the operational condition of nanoscopic motors with that of macroscopic counterparts.

Energy scales

For biomolecules whose sizes are on the nanometer scale, the effect of thermal noise ($k_BT \approx 4 \times 10^{-21} J = 4pN \cdot nm$) on the molecule is no longer negligible because the energy scale of individual non-covalent bond interactions ($\sim \mathcal{O}(1)\ k_BT$) is of the same order. Dominance of entropy is ubiquitous in soft matters such as polymer, colloids, bubbles and biomolecules. Due to free energy barriers that are created by incomplete cancellation between enthalpy and entropy (1), conformational transitions of biopolymers occur cooperatively. If the kinetic barrier associated with a transition is too large to overcome using thermal fluctuations, free energy borrowed from the chemical potential of molecular fuel can make the conformational change biologically accessible. Actively adopting the environmental noise to induce functional motion is one of the key design principles unique to biological motors. In contrast, for macroscopic motors that operate through tight couplings among a multitude of rigid bodies, the thermal fluctuations are rather a nuisance to achieve better accuracy and precision (2). An integral part of this review lies in understanding the *soft* mechanics of biological motors.

Thermodynamics

Carnot engines that exemplifies the thermodynamics in the macroworld extract mechanical work (W) by accepting heat Q_h from a hot reservoir at temperature T_h and discarding the remaining heat Q_c into a cold reservoir at T_c (see Fig. S1a for gasoline engine as an example of practical heat engine cycle). The maximal work, which amounts to the heat transfer between the

two reservoirs $W_{max} = Q_h - Q_c$, is extracted when an engine is operated *quasi-statically*without dissipating heat. Real heat engines, however, do not adopt the quasi-static operation for all practical purposes; some amount of heat dissipation is inevitable. As a result, the extracted work is always smaller than the heat transfer ($W \leq Q_h - Q_c$), thus the thermodynamic efficiency for the engine is bounded by $\eta_{Carnot} = (Q_h - Q_c)/Q_h = 1 - T_c/T_h$, where $Q_h/Q_c = T_h/T_c$. To increase the efficiency, macroscopic machines are designed to minimize heat dissipation by lubricating the parts of the machine that are prone to produce friction.

In contrast to the thermodynamic conditions imposed on macroscopic engines, molecular motors operate under isothermal and highly dissipative environments; thus an thermodynamic cycle with two distinct isotherms as in the Carnot engine is not applicable for biological motors. Instead, conformational changes of internal structure can be linked to the motor cycle (see the main text for the discussion using polyazopeptide and kinesin).

Low Reynolds number environment

Reynolds number, defined as $Re = \rho va/\eta$, is equivalent to the ratio of inertial force ($F_{inertial} \propto \rho a^2 v^2$) to viscous force ($F_{viscous} \propto \eta av$), where ρ and η are the density and viscosity of media, and a and v are the size and speed of an object in motion (3). Significant variation of Re values implies that there is fundamental difference in the dynamics. The Reynolds numbers associated with motions at both atomic and macroscopic scales satisfy $Re \gg 1$. A macroscopic object ($a \sim cm$) moving $v \sim cm/s$ through water with the kinematic viscosity $\eta/\rho \approx 10^{-2}\ cm^2/sec$ will have $Re \sim 10^2 \gg 1$; At atomic scales, the surrounding media looks discrete, so the dynamics such as vibrational motion of hydrogen bonds occurs essentially in vacuum ($\eta/\rho \approx 0$), thus $Re \gg 1$ and inertial forces are dominant. In contrast, for a typical protein, whose size is $a \sim nm$, the time scales associated with domain motions, such as looping dynamics and beta sheet formation is $\lesssim (0.1 - 1)$ μsec (4); thus the typical velocity of motion is $v \approx 0.5\ cm/sec$, resulting in $Re \approx (10^{-5} - 10^{-6}) \ll 1$. The estimated value of Re indicates that even for a large biomolecule like the ribosome ($a \sim 20\ nm$) the molecular motions occur in a very low Re regime. In the $Re \ll 1$ regime, reciprocal motions employed by a swimmer in macroworld do not gain propulsion from the fluid surrounding the molecule. Molecular motors, therefore, have to adopt an entirely different strategy from the one in the macroworld, to break time reversal and translational symmetry (3).

The above mentioned basic constraints enable us to draw a few general conclusions about molecular motors: (i) Due to constant exposure to noisy environment and structural flexibility, the deterministic description using the rigid body motion of macroscopic objects is no longer valid to describe the probabilistic nature of dynamics of biological systems. (ii) Unlike macroscopic heat engines that extract work out of heat reservoirs, molecular motors transduce chemical energy into mechanical work by exploiting the changes of molecular topology (5). Small and large structural adaptations are the vital components of free energy transduction. (iii) For biological motors bombarded by thermal noise, the distinction between the system of interest and surroundings is not obvious since system-bath interactions are non-negligible. Furthermore, unlike macroscopic heat engines, the heat dissipated due to friction can also be replenished by the thermal energy from the solvent, which is a qualitative description of fluctuation-dissipation theorem. Instead of minimizing the heat dissipation, molecular machines actively utilize molecular fluctuations due to thermal noise. (iv) To produce uni-directional transport or rotational dynamics under low Reynolds number conditions, isotropy in the diffusive dynamics has to be broken.

Besides the general principles of molecular motors, understanding individual motors requires more specific knowledge on their architecture and related dynamics (6). To this end, we explore the details of design principles in biological motors by focusing on one of the best studied molecular motors, kinesin-1.

Nonequilibrium steady state thermodynamics

In discussing the action of molecular motors, it should be remembered that each state of the molecular motor along a biochemical cycle is in nonequilibrium steady state (NESS); in principle, one should not use the notion of equilibrium thermodynamics. Nevertheless, an extended form of the thermodynamics for NESS has long been suggested and recently revisited (7, 8). In the NESS formalism, the second law of steady state thermodynamics reads $T\Delta S \geq Q_{ex}$ or $\langle W_{ex} \rangle \geq \Delta F$ where ΔS is the difference of Shannon entropy between the two states and Q_{ex} (excess heat) is the total heat (Q_{tot}) subtracted by the housekeeping heat (Q_{hk}) generated in an infinitely slow process, where Q_{hk} is the heat required to maintain constant non-zero flux between the two steady states (9). According to the NESS thermodynamics of open systems, the concentrations of four NT states, held constant as a

source and sinks of the system, provide a constant chemical potential difference that drives the biochemical cycle; one can define an effective free energy difference between two steady states by using the ratio of the forward and backward rate constants measured at near-equilibrium condition (7, 8, 10, 11).

ATP-Wait state

At high [ATP]($\approx$ 1 mM) when the leading head is bombarded by ATP molecules every 0.5 ms (bi-molecular rate constant for ATP binding is $k^o_{ATP} = 2.0 \pm 0.8 \mu M^{-1} s^{-1}$), the rate limiting step for the kinesin cycle is the hydrolysis or Pi-release from the trailing head ($\approx$ 10 ms). In contrast, at [ATP]$\approx$ $1\mu M$, the leading head is inaccessible to ATP for 0.5 sec ($\gg$ 10 ms) during which all the processes including ATP hydrolysis, Pi release take place, thus the ATP binding becomes the rate limiting step. Therefore, among the series of kinesin configurations, the ADP-ϕ state becomes the rate limiting configuration at low [ATP]. It is worth reviewing the series of recent studies, led by several experimental groups, to address an intriguing question as to whether kinesins in ADP-ϕ state wait for ATP binding in one head (1HB) or two head bound (2HB) form (12–15).

By analyzing the concentration of $\alpha\beta$-tubulin and kinesin-1 at various nucleotide conditions Alonso *et al.* showed that stoichiometry of kinesin-1 to tubulin is 1:1 under ADP only condition but this changes to 1:2 in the presence of AMP-PNP (ATP-analog) (12). The 1:2 stoichiometry is consistent with the information of MT affinity summarized in the Table 1 (main text) since both NT-free and AMP-PNP states strongly bind the MT. The 1:1 stoichiometry under ADP only condition results from a kinesin conformation in which one head is in NT-free state that binds MT strongly while the other head is still in ADP state. Based on the cryo-EM map, Alonso *et al.* proposed a structure of ATP-wait state in which the tethered head parks on top of its partner head, blocking its MT-binding motifs, and further inferred that the ATP binding to the MT-bound NT-free kinesin head unblocks the MT binding motifs of the tethered head, enabling the kinesin-tubulin interaction.

Alonso *et al.*'s proposal for ATP-wait conformation (12) was examined by the more quantitative analysis using sm-FRET, which directly probed the "distance" between the two kinesin heads parked on MTs. In reference to the sm-FRET distributions for 2HB and 1HB structures, the latter of which were prepared using mutant heterodimeric kinesin, Mori *et al.* concluded

that kinesin waits ATP in 2 HB state at high [ATP]($\approx 1mM$) and in 1 HB state at low [ATP]($\approx 2\mu M$). At low [ATP], FRET time trace indicates that a kinesin step has a short-lived 2HB state, which then undergoes a transition to a long-lived 1HB state. Also, at low [ATP] the detached head is on average located rearward relative to the NT free MT-bound head (13).

The picture of ATP-wait state by Mori *et al.* (13) was further elaborated by Asenjo *et al.* who probed the mobility of tethered kinesin head by using fluorescence polarization microscopy (FPM) (14). The FPM showed that the unbound head is highly mobile. Especially, the high mobility of detached head at low [ATP] rules out the parked configuration of the tethered head proposed by Alonso *et al.* In fact, the PMF calculated for the head tethered to a disordered NL (Fig. 2b left) succinctly demonstrates the space explored by the tethered head in 1HB state (16). The recognition of the next binding site is promoted only after the NL docking. The NL zippered state of the MT-bound head restricts the search space of the tethered head and facilitate the tethered head to locate the next MT-binding site.

Most recently, Guydosh *et al.* conducted an optical tweezers experiment to provide a direct probe of the ATP-wait stage at low ATP concentration ($=2\mu M$) (15). Instead to the stalk region, they tethered a micro-bead to one of the two kinesin heads and probed its dynamics. In response to the external load that rapidly alternate between hindering (-1.7 pN) and assisting ($+1.7$ pN) phases with 14 ms time interval, the kinesin head showed signals swinging back and forth, which indicate that the kinesin is in 1HB state. Such a swinging motion would have not been possible if the kinesin had been in 2HB state. Under the assisting load ($+1.7$ pN) the tethered head showed overshoot step that reaches ~ 23 nm and recovery step (~ -7 nm) upon ATP binding to the MT-bound head. The decrease of overshoot dwell with increasing ATP concentrations suggests that the recovery step is induced by ATP binding. Based on the swinging motion that freely occurs with no signature of disruption even under ± 1.7 pN load, Guydosh *et al.* concluded that the ATP wait stage of kinesin is 1 HB state. The possibility of 2 HB state was essentially precluded based on the estimate that the binding affinity of weakly bound ADP state is even less than thermal energy k_BT (If the location of transition state is assumed to be 2 nm, unbinding energy is 1.7 pN $\times$ 2 nm $\approx$ 3.4 pN$\cdot$nm$<$ 4.14 pN$\cdot$nm). The conclusion against 2HB state in Guydosh *et al*'s study contradicts to Mori *et al.* and Asenjo *et al.*'s studies (13, 14). However, the time interval of alternating load ($\sim$ 14 ms) used in the experiment is still longer than the average dwell time of kinesin at saturating ATP condition under which 2HB state is shown to be dominant in ADP-ϕ state in Refs. (13, 15). A signature of disruption missing

under 1.7 pN load may be due to the relatively long time interval during which the spontaneous dissociation of ADP containing tethered head can occur from the trailing head position in MTs.

Figure Legends

Figure S1.

Macroscopic heat engines. **a.** Thermodynamic cycle of Carnot engine. **b.** The thermodynamic cycle of idealized gasoline engine (Otto cycle), which consists of (i) compression of vapor (adiabatic compression) → (ii) combustion of the gasoline at the chamber with constant volume (isochoric heating) → (iii) power stroke (adiabatic expansion) → (iv) isochoric cooling. At the step (ii) heat is absorbed to the engine but unlike Carnot cycle the temperature involving this step is not constant. Therefore, the absorbed heat should be integrated over the varying temperatures. By assuming an ideal gas for the gasoline vapor, the maximum thermodynamic efficiency of Otto cycle is obtained with the ratio of volume before and after the compression, and two heat capacities ($c_p = (dQ/dT)_p$, $c_v = (dQ/dT)_v$), $\eta_{Otto} = 1 - (V_f/V_i)^{\frac{c_p - c_v}{c_v}}$. In practice, the engine needs to be supplied with fresh gasoline vapor and the compression cannot be made by the single engine alone. Thus, to realize the steps (i) and (iv) the piston of engine is operated in concert with others.

Figure S2.

Kinesin structure and its conformational changes with various NT states. **a**. Details of kinesin structure. The kinesin monomer is structurally divided into three regions: the head domain (or motor domain) (residues 2-323), the neck-linker (NL) (residues 324-338: β9, β10), and the neck-helix (residue 339-: α7). With respect to the central β-sheets (β1, β8, β3, β7, β6, β4) the head domain is divided into two sides; one side, made of α4, α5, α6, L8, L11, and L12, is used to bind MTs, and the other side has NT-binding pocket surrounded by the structural motifs consisting of the P-loop (N1) (86-93), switch-I (N2) (199-204), switch-II (N3) (232-237), and N4. Structural changes of kinesin along the biochemical cycle of ATP binding, hydrolysis, Pi and ADP releases are shown in **b** and **c**. **b**. The configurations of structural motifs surrounding the nucleotide binding pocket in AMPPNP (ATP analog) state (PDB id : 1i6i) (enclosed in magenta box), in ADP-AlF_x (ADP·Pi analog) state (PDB id : 1vfx) (blue box), and in ADP-V_i (ADP analog) state (green box) (17). The orientation of α4 (yellow helix) changes

upon Pi release. **c**. Schematics showing the changes of NL configuration and kinesin-MT interaction indicated with red and blue arrows, respectively.

Figure S3.

ATP-wait state at two different ATP concentrations. At high ([ATP]=1mM) and low ([ATP]=1 μM) ATP concentrations, kinesins wait for ATP in 2HB and 1HB states, respectively. At 1HB state, the cartoon illustrate a substantial fluctuation in the tethered head (14).

References

1. Onuchic, J. N., and P. G. Wolynes, 2004. Theory of protein folding. *Curr. Opin. Struct. Biol.* 14:70–75.

2. Oosawa, F., 2000. The loose coupling mechanism in molecular machines of living cells. *Genes to Cells* 5:9–16.

3. Purcell, E. M., 1977. Life at low Reynolds number. *Am. J. Phys.* 45:3–11.

4. Thirumalai, D., and C. Hyeon, 2005. RNA and Protein folding: Common Themes and Variations. *Biochemistry* 44:4957–4970.

5. Hugel, T., N. B. Holland, A. Cattani, L. Moroder, M. Seitz, and H. E. Gaub, 2002. Single-Molecule Optomechanical Cycle. *Science* 296:1103–1106.

6. Alberts, B., and R. Miake-Lye, 1992. Unscrambling the puzzle of biological machines: the importance of the details. *Cell* 68:415.

7. Hill, T. L., 1989. Free Energy Transduction and Biochemical Cycle Kinetics. Springer-Verlag.

8. Beard, D. A., and H. Qian, 2008. Chemical Biophysics. Cambridge University Press.

9. Hatano, T., and S. Sasa, 2001. Steady-state thermodynamics of Langevin systems. *Phys. Rev. Lett.* 86:3463–3466.

10. Hyeon, C., and J. N. Onuchic, 2009. Proteins: Energy, Heat and Signal Flow, CRC Press, chapter Energy balance and Dynamics of Kinesin Motors, 3–22.

11. Hyeon, C., S. Klumpp, and J. N. Onuchic, 2009. Kinesin's backsteps under mechanical load. *Phys. Chem. Chem. Phys.* 11:4899–4910.

12. Alonso, M. C., D. R. Drummond, S. Kain, J. Hoeng, L. Amos, and A. Cross, 2007. An ATP Gate Controls Tubulin Binding by the Tethered Head of Kinesin-1. *Science* 316:120–123.

13. Mori, T., R. D. Vale, and M. Tomishige, 2007. How kinesin waits between steps. *Nature* 450:750–754.

14. Asenjo, A. B., and H. Sosa, 2009. A mobile kinesin-head intermediate during the ATP-waiting state. *Proc. Natl. Acad. Sci. USA* 106:5657–5662.

15. Guydosh, N. R., and S. M. Block, 2009. Direct observation of the binding state of the kinesin head to the microtubule. *Nature* 461:125–128.

16. Hyeon, C., and J. N. Onuchic, 2007. Mechanical control of the directional stepping dynamics of the kinesin motor. *Proc. Natl. Acad. Sci. USA* 104:17382–17387.

17. Nitta, R., M. Kikkawa, Y. Okada, and N. Hirokawa, 2004. KIF1A alternatively uses two loops to bind microtubules. *Science* 305:678–683.

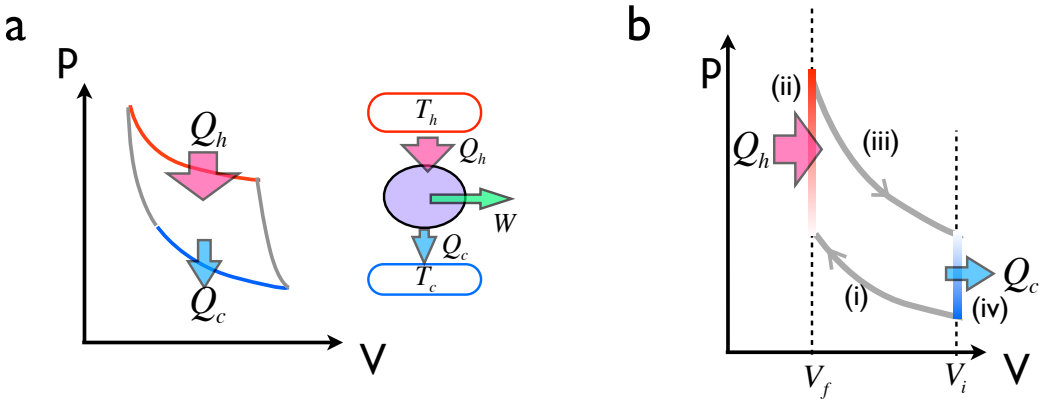

Figure S1:

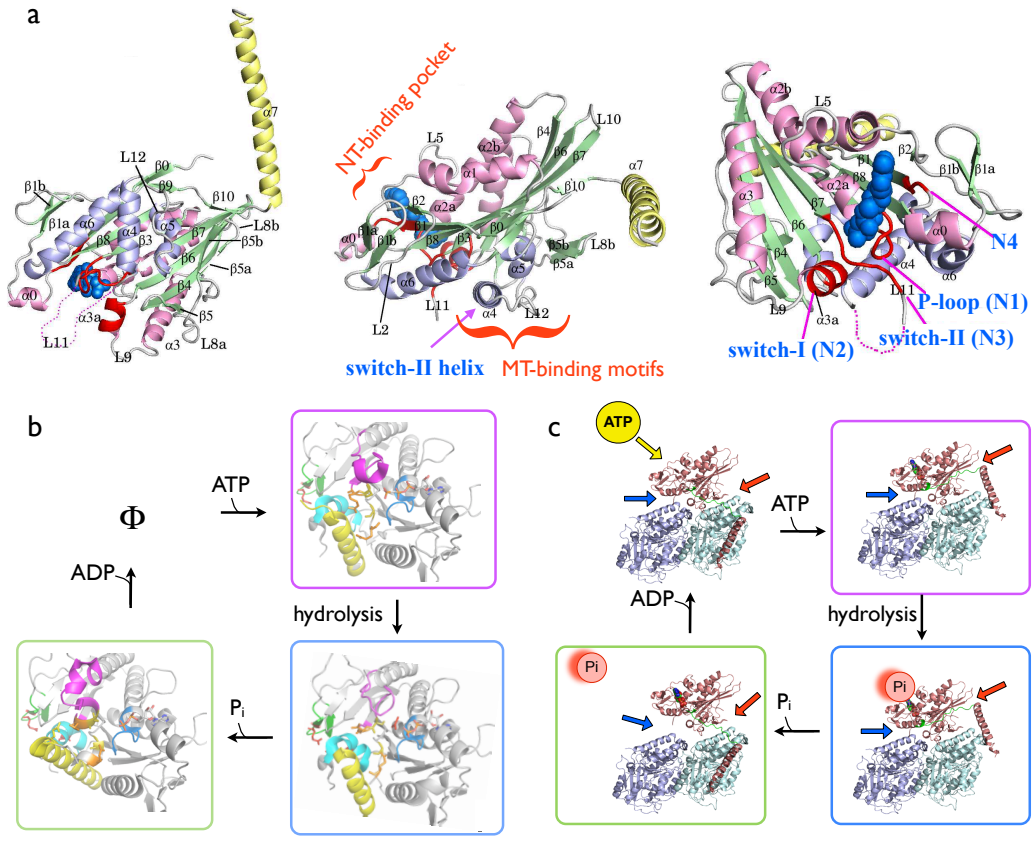
a
NT-binding pocket
switch-II helix
MT-binding motifs
N4
P-loop (N1)
switch-I (N2)
switch-II (N3)
b
ATP
Φ
ADP
hydrolysis
Pi
c
ATP
ADP
hydrolysis
Pi
Pi

Figure S2:

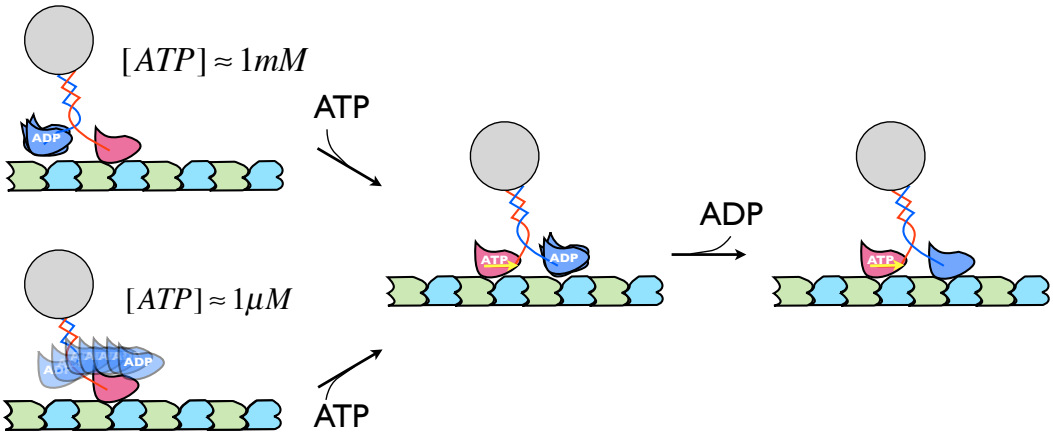

Figure S3: